https://doi.org/10.1007/s11467-022-1218-6

RESEARCH ARTICLE

A multi-band atomic candle with microwave-dressed Rydberg atoms

Yafen Cai[1,*], Shuai Shi[1,*], Yijia Zhou[2,*], Jianhao Yu[1], Yali Tian[1], Yitong Li[1], Kuan Zhang[1], Chenhao Du[1], Weibin Li[3,†], Lin Li[1,‡]

[1]MOE Key Laboratory of Fundamental Physical Quantities Measurement, Hubei Key Laboratory of Gravitation and Quantum Physics, PGMF, Institute for Quantum Science and Engineering, School of Physics, Huazhong University of Science and Technology, Wuhan 430074, China

[2]Graduate School of China Academy of Engineering Physics, Beijing 100193, China

[3]School of Physics and Astronomy and Centre for the Mathematics and Theoretical Physics of Quantum Non-equilibrium Systems, University of Nottingham, Nottingham, NG7 2RD, UK

[*]These authors contributed equally.

Corressponding authors. E-mail: [†]weibin.li@nottingham.ac.uk, [‡]li_lin@hust.edu.cn

Received June 27, 2022; accepted October 12, 2022

Supporting Information

Theoretical model

Atomic candle signal. The polarization of the atoms in the medium is of great importance as we study the atomic candle signal (ACS) and the error signal. The polarization induced by the transition $|g\rangle \rightarrow |e\rangle$, will enter the Maxwell's equation as a source term. In this work, our atom gas is dilute ($\sim 3 \times 10^{11}$ cm^{-3}) in the sense that the interactions between Rydberg atoms are negligible. Therefore, we use a single-atom model to describe the atom-light interaction. The electric field of the probe laser, $\mathcal{E}_p(t,z)$, under the slow varying field approximation is governed by [1, 2]

$$\frac{\partial \mathcal{E}_p}{\partial z} + \frac{1}{c}\frac{\partial \mathcal{E}_p}{\partial t} - i\frac{\nu_p}{2c\epsilon_0}\mathcal{N}\mu_{ge}\rho_{ge} = 0, \tag{S.1}$$

where the direction of the propagation is along z-axis, ϵ_0 is the vacuum permittivity, ν_p is the angular frequency of the probe laser, μ_{ge} is the dipole moment of the transition $|g\rangle \rightarrow |e\rangle$, and $\mathcal{N}$ is the total atom density. In a homogeneous system, the transmission, T, through a vapor cell with length being L follows the Beer-Lambert law [3]

$$T = \exp\left[-\frac{4\pi\mathcal{N}L|\mu_{ge}|^2}{\hbar\epsilon_0\lambda_p\Omega_p}\mathrm{Im}\,\rho_{ge}\right], \tag{S.2}$$

where λ_p and Ω_p are the wavelength and Rabi frequency of the probe laser. Density matrix ρ of the atoms is governed by the master equation ($\hbar \equiv 1$),

$$\dot{\rho} = \mathcal{L}[\rho] = -i[H,\rho] + \mathcal{D}[\rho], \tag{S.3}$$

where

$$H = -\Delta_p\sigma_{ee} - (\Delta_p + \Delta_c)(\sigma_{r_1r_1} + \sigma_{r_2r_2}) + \frac{\Omega_p}{2}(\sigma_{ge} + \sigma_{eg}) + \frac{\Omega_c}{2}(\sigma_{er_1} + \sigma_{r_1e}) + \frac{\Omega_{\mathrm{MW}}}{2}(\sigma_{r_2r_1} + \sigma_{r_1r_2}) \tag{S.4}$$

and

$$\mathcal{D}[\rho] = \sum_{ij} \frac{\gamma_{ij}}{2}\left(2\sigma_{ij}\rho\sigma_{ji} - \{\sigma_{ii}, \rho\}\right)$$

$$= \begin{pmatrix} \gamma_e\rho_{ee} + \gamma_{r_1}\rho_{r_1r_1} + \gamma_{r_2}\rho_{r_2r_2} & -\frac{1}{2}\Gamma_e\rho_{ge} & -\frac{1}{2}\Gamma_{r_1}\rho_{gr_1} & -\frac{1}{2}\Gamma_{r_2}\rho_{gr_2} \\ -\frac{1}{2}\Gamma_e\rho_{eg} & -\gamma_e\rho_{ee} & -\frac{1}{2}(\Gamma_e + \Gamma_{r_1})\rho_{er_1} & -\frac{1}{2}(\Gamma_e + \Gamma_{r_2})\rho_{er_2} \\ -\frac{1}{2}\Gamma_{r_1}\rho_{r_1g} & -\frac{1}{2}(\Gamma_e + \Gamma_{r_1})\rho_{r_1e} & -\gamma_{r_1}\rho_{r_1r_1} & -\frac{1}{2}(\Gamma_{r_1} + \Gamma_{r_2})\rho_{r_1r_2} \\ -\frac{1}{2}\Gamma_{r_2}\rho_{r_2g} & -\frac{1}{2}(\Gamma_e + \Gamma_{r_2})\rho_{r_2e} & -\frac{1}{2}(\Gamma_{r_1} + \Gamma_{r_2})\rho_{r_2r_1} & -\gamma_{r_2}\rho_{r_2r_2} \end{pmatrix} \tag{S.5}$$

The atomic projection operators are $\sigma_{ij} = |i\rangle\langle j|$, with i and j referring to $|g\rangle, |e\rangle, |r_1\rangle, |r_2\rangle$ states. Δ_p and Δ_c are the detuning of the probe and control lasers,

$$\Delta_{p,c} = \nu_{p,c} - \omega_{p,c}, \tag{S.6}$$

where $\nu_{p,c}$ are the angular frequencies of the probe and control lasers, and $\omega_{p,c}$ are the on-resonance angular frequencies of transitions $|5S_{1/2}\rangle \rightarrow |5P_{1/2}\rangle$ and $|5P_{1/2}\rangle \rightarrow |nD_{3/2}\rangle$. The atomic states are $|g\rangle = |5S_{1/2}\rangle$ $|e\rangle = |5P_{1/2}\rangle$, $|r_1\rangle = |nD_{3/2}\rangle$, and $|r_2\rangle = |(n+1)P_{1/2}\rangle$, where all the magnetic quantum numbers $|m_j| = 1/2$ as the lasers and microwave (MW) are linearly polarized. γ_e, γ_{r_1}, and γ_{r_2} are spontaneous decay rates of the corresponding states, and $\Gamma_e, \Gamma_{r_1}, \Gamma_{r_2}$ are dephasing rates resulting from the spontaneous decay, collisions and interactions between atoms.

The Rabi frequencies Ω_p and Ω_c are calculated with the parameters of the laser beams including their powers, P, and $1/e^2$ waists, w_0. The electric field of the laser beam is $E = \sqrt{4P/(\pi\varepsilon_0 c w_0^2)}$, and the corresponding Rabi frequency is $\Omega = \mu \cdot E/\hbar$, where μ is the dipole moment of the corresponding transition. For the π-transition $|5S_{1/2}\rangle \rightarrow |5P_{1/2}\rangle, |\mu_{ge}| = 1.727ea_0$(Ref. [4]) We calculate dipole moments involving Rydberg states using the Alkali-Rydberg-Calculator [5, 6], for $|5P_{1/2}\rangle \rightarrow |53D_{3/2}\rangle$, $|\mu_{er_1}| = 0.0104ea_0$, and for $|53D_{3/2}\rangle \rightarrow |54P_{1/2}\rangle$ $|\mu_{r_1r_2}| = 1694ea_0$. Given the parameters of the probe beam (795 nm) being $P = 4\ \mu$W, $w_0 = 136\ \mu$m, one obtains its average Rabi frequency $\Omega_p = 2\pi \times 7.6$ MHz. As for the control laser (474 nm), $P = 78$ mW, $w_0 = 110\ \mu$m, its Rabi frequency is $\Omega_c = 2\pi \times 7.3$ MHz.

The dissipation operator $\mathcal{D}[\rho]$ consists of spontaneous decay and dephasing terms. The spontaneous decay rate of the excited state is $\gamma_e = 2\pi \times 5.746$ MHz(ref. [7]), and for the Rydberg states $|r_1\rangle = |53D_{3/2}\rangle$ and $|r_2\rangle = |54P_{1/2}\rangle$ $\gamma_{r_1} = 2\pi \times 2.007$ kHz, and $\gamma_{r_2} = 2\pi \times 1.492$ kHz [5, 6] The dephasing rates Γ_e, Γ_{r_1}, and Γ_{r_2} depend on the environment and are free parameters to fit the experimental data [8-11]. In this work, to our best fit, we find $\Gamma_e = 2\pi \times 6.0$ MHz, $\Gamma_{r_1} = 2\pi \times 0.5$ MHz and $\Gamma_{r_2} = 2\pi \times 3.0$ MHz for the Rydberg states $|r_1\rangle = |53D_{3/2}\rangle$ and $|r_2\rangle = |54P_{1/2}\rangle$.

A modulation at frequency ω_m is applied to the detuning of the probe laser (modulation amplitude δ_m), such that the master equation is appended with an additional modulation term,

$$[\dot{\rho}]_{\mathrm{mod}} = \mathrm{i}\big[\delta_m \sin(\omega_m t)\big(\sigma_{ee} + \sigma_{r_1 r_1} + \sigma_{r_2 r_2}\big), \rho\big], \tag{S.7}$$

which can be also written as

$$[\dot{\rho}]_{\mathrm{mod}} = \big(\tilde{\mathcal{L}} e^{\mathrm{i}\omega_m t} - \tilde{\mathcal{L}} e^{-\mathrm{i}\omega_m t}\big)\rho\ . \tag{S.8}$$

Since the modulation is monochromatic, we assume that the quasi-steady-state solution to ρ and the Liouville operator $\mathcal{L}$ can be expanded as the sum of a series of oscillatory parts with integer times of the modulation frequency, such that

$$\rho(t) = \sum_{n=-\infty}^{+\infty} \rho^{(n)} e^{\mathrm{i}n\omega_m t} \tag{S.9}$$

and the master equation can be written as a series of algebraic equations

$$\begin{aligned} & \mathrm{i}\sum_{n=-\infty}^{+\infty} n\omega_m \rho^{(n)} e^{\mathrm{i}n\omega_m t} \\ = \ & \big(\mathcal{L} + \tilde{\mathcal{L}} e^{\mathrm{i}\omega_m t} - \tilde{\mathcal{L}} e^{-\mathrm{i}\omega_m t}\big) \sum_{n=-\infty}^{+\infty} \rho^{(n)} e^{\mathrm{i}n\omega_m t}\ . \end{aligned} \tag{S.10}$$

Then we obtain a recurrence equation for ρ_n,

$$(\mathcal{L} - \mathrm{i}n\omega_m \mathcal{I})\rho^{(n)} + \tilde{\mathcal{L}}\rho^{(n-1)} - \tilde{\mathcal{L}}\rho^{(n+1)} = 0\ . \tag{S.11}$$

If we truncate the series of $\rho^{(n)}$ at $n = 2$, i.e., $\rho^{(\pm 3)} = 0$, which will be shown as necessary in the dynamical simulation, we find that the solution to $\rho^{(0)}$ follows $\mathcal{K}_0 \rho^{(0)} = 0$, where

$$\begin{aligned} \mathcal{K}_0 &= \mathcal{L}_0 + \tilde{\mathcal{L}}\mathcal{K}_1 + \tilde{\mathcal{L}}\mathcal{K}_{-1}, \\ \mathcal{K}_{\pm 1} &= \mp\big(\mathcal{L}_{\pm 1} + \tilde{\mathcal{L}}\mathcal{K}_{\pm 2}\big)^{-1}\tilde{\mathcal{L}}, \\ \mathcal{K}_{\pm 2} &= \mp\mathcal{L}_{\pm 2}^{-1}\tilde{\mathcal{L}}, \\ \mathcal{L}_n &= \mathcal{L} - \mathrm{i}n\omega_m \mathcal{I}. \end{aligned}$$

The other terms can be generated accordingly, such that $\rho^{(n)} = \mathcal{K}_n \rho_{n-1}$ for $n > 0$ and $\rho^{(n)} = \mathcal{K}_n \rho_{n+1}$ for $n < 0$.

The first step, $\mathcal{K}_0 \rho^{(0)} = 0$, can be resolved with the direct method or eigenstate method [12]. In this work, we use the direct method. First, we vectorize the density matrix, and the superoperator $\mathcal{K}_0$ has a matrix representation. Then we make use of the boundary condition that $\mathrm{Tr}\big[\rho^{(0)}\big] = 1$. We vectorize the identity matrix $\mathcal{I}$ to a row vector, then add it to the first row of $\mathcal{K}_0$ yielding $\mathcal{K}_0'$. Finally, the steady state can be directly solved as $\rho_0 = \mathcal{K}_0'^{-1} b$, where $b = (1,0,0,\cdots)^{\mathsf{T}}$.

To verify the validity of this perturbation approximation, we make a benchmark compared with the numerical simulation of the original master equation. We let the detuning of the probe laser to be $\tilde{\Delta}_p(t) = \Delta_p + \delta_m \sin(\omega_m t)$ where $\Delta_p = 2\pi \times 8$ MHz, and the modulation amplitude is $\delta_m = 2\pi \times 1$ MHz, and the modulation frequency $\omega_m = 2\pi \times 50$ kHz. The perturbation is truncated at the second order. We change the MW field amplitude to be 2, 8 and 20 mV $\cdot$ cm^{-1}, and plot the imaginary part of ρ_{ge} as shown in Fig. S1, showing excellent agreement.

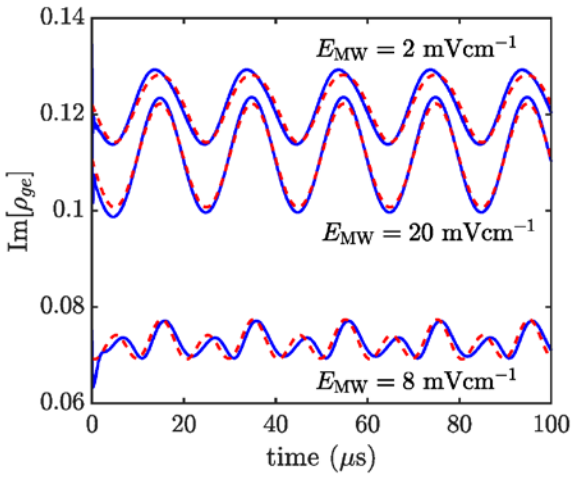

Fig. S1 Imaginary part of ρ_{ge} using the perturbation approximation (dashed red curves) and real-time simulation (solid blue curves). The MW amplitudes are $2, 8, 20\ \mathrm{mV \cdot cm^{-1}}$.

When the MW field amplitude deviates from the target value, whether in the weak field ($E_{\mathrm{MW}} = 2\ \mathrm{mV \cdot cm^{-1}}$) or strong field ($E_{\mathrm{MW}} = 20\ \mathrm{mV \cdot cm^{-1}}$) regime, the evolution of $\rho(t)$ is monochromatic. However, when the MW field amplitude approaches the target value, the dynamics of the probe laser becomes dichromatic. Our simulation shows that the perturbation truncated at the second order is necessary to reveal the dynamics near the target MW field amplitude, and is also sufficient to capture the major features. The most significant difference between the perturbation and numerical simulation is a phase shift.

The Doppler effect is taken into account by modifying the detuning $\Delta_{p,c} \to \Delta_{p,c} + \mathbf{k}_{p,c} \cdot \mathbf{v}$, where $|\mathbf{k}_{p,c}| = 2\pi/\lambda_{p,c}$ and $\mathbf{v}$ is the velocity of the atoms, and only v_z component (parallel to the propagating direction of the lasers) is significant since the Doppler shift caused by the MW field is negligible. The thermally averaged density matrix is

$$\langle\rho\rangle_{\mathrm{th}} = \sqrt{\frac{m}{2\pi k_B T_{emp}}} \int \rho(v_z) \exp\left(-\frac{m v_z^2}{2 k_B T_{emp}}\right) \mathrm{d}v_z \ , \tag{S.12}$$

where m is the mass of atom, k_B is Boltzmann's constant and T_{emp} is temperature in Kelvin.

Error signal. In order to remove the Doppler background and enhance the signal-to-noise ratio, we obtain the ACS via a balanced detector (Thorlabs PDB450A). The transmission is calculated via Eq. (S.2), where ρ_{ge} only takes the zeroth order into consideration, and

$$\mathrm{ACS} = T_{\mathrm{probe}} - T_{\mathrm{reference}}. \tag{S.13}$$

In order to obtain the error signal for feedback control, the ACS is modulated accordingly, which, in principle, contains a series of oscillating modes whose frequencies are the integer times of the modulation frequency. The previous experiments using ground states modulate MW field amplitude. In comparison, we modulate the frequency of the probe laser, such that the MW field amplitude is undisturbed. In our demonstration, the modulation frequency is $\omega_m = 2\pi \times 50$ kHz, and the modulation amplitude is $\delta_m = 2\pi \times 1$ MHz. The detected ACS is then demodulated to pick up its modulation-frequency component, which serves as the error signal.

The error signal can be derived from Eq. (S.2) with Jacobi-Anger expansion. Since $\rho_{ge}(t) = \rho^{(0)} + \rho^{(1)} e^{\mathrm{i}\omega_m t} + \rho^{(-1)} e^{-\mathrm{i}\omega_m t} + \cdots$, we can also fast Fourier transform $T(t)$ to $\tilde{T}(n\omega_m)$, where $n = 0, \pm 1, \cdots$. The demodulation process picks up the first-order term, $\tilde{T}(\omega_m)$, as the error signal which reads

$$\text{Error signal} = \bar{T} \frac{B}{A} I_1\left(-\frac{4\pi \mathcal{N} L |\mu_{ge}|^2}{\hbar \epsilon_0 \lambda_p \Omega_p} A\right), \tag{S.14}$$

where $\bar{T}$ is the zero-order term obtained by time averaging in the experiment, and $I_1(x)$ is the modified Bessel function of the first kind, $A = \sqrt{\left|\rho_{ge}^{(1)}\right|^2 + \left|\rho_{ge}^{(-1)}\right|^2 - 2\mathrm{Re}\left[\rho_{ge}^{(1)}\rho_{ge}^{(-1)}\right]}, B = \mathrm{Re}\left[\rho_{ge}^{(1)} - \rho_{ge}^{(-1)}\right]$.

Then we show that the error signal is approximately equal to the derivative of the ACS. First, when the modulation amplitude is small, the argument inside I_1 of Eq. (S.14) is small, $I_1(x) \approx x$, and the error signal is only proportional to $B = \mathrm{Re}\left[\rho_{ge}^{(1)} - \rho_{ge}^{(-1)}\right]$. Second, substituting $n = 0$ into Eq. (S.11), we have

$$\tilde{\mathcal{L}}\left(\rho^{(1)} - \rho^{(-1)}\right) = \mathcal{L}_0\rho^{(0)} \,. \tag{S.15}$$

Third, note that $\tilde{\mathcal{L}}$ is diagonal, which leads to the ge-component of the LHS equal to $-\mathrm{i}\delta_m\left(\rho_{ge}^{(1)} - \rho_{ge}^{(-1)}\right)$. The RHS is approximately equal to $\tilde{\mathcal{L}}(\mathcal{L}_1^{-1} - \mathcal{L}_{-1}^{-1})\tilde{\mathcal{L}}\rho^{(0)}$ (expand to the first-order perturbation), whose ge-component is also proportional to $\rho_{ge}^{(0)}$. Therefore, we conclude that the ACS is proportional to the imaginary part of $\rho_{ge}^{(0)}$, and the error signal is proportional to its real part. According to Kramers-Kronig relation, the error signal is roughly proportional to the derivative of ACS when the latter approaches its maximum.

There are two significant consequences of the Doppler effect. First, the measured spectral distance between the two EIT peaks is shrunk by a factor λ_c/λ_p. This factor is a high-temperature limit, and it nearly a constant for T>100 K. Second, the linewidths of the EIT windows are broadened, which degrades the performance of the atomic candle, because the slope of the error signal is inverse of the linewidth.

Furthermore, we remark that the linewidth of the EIT is affected by the temperature. We calculated the full width at half maximum (FWHM) of the EIT window for $|g\rangle \rightarrow |e\rangle \rightarrow |r_1\rangle$ (Fig. S2). We found that the FWHM can be fitted numerically and is scaled with $\propto T_{\mathrm{emp}}^{1/4}$.

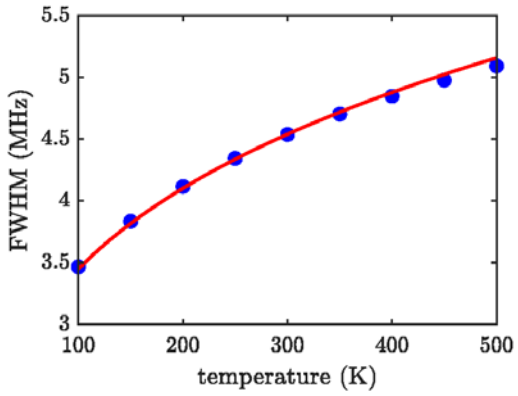

Fig. S2 The blue dots shown the calculated FWHMs of the EIT window versus different temperature. The solid red line is the fitting of FWHM $\propto T_{emp}^{1/4}$.

Modulation bandwidth. The modulation frequency is essential for determining the stabilization bandwidth of the Rydberg atomic candle. It is favored to achieve high frequency modulation while the error signal is sufficiently strong for feedback control. We define the error signal slope which is equal to differentiating the error signal over the MW field amplitude at the transparency window. The error signal slopes as a function of modulation frequency are shown in Fig. S3. We fix the detuning of the probe laser to be $\Delta_p = 2\pi \times 10$ MHz, and the modulation amplitude to be $\delta_m/(2\pi) = 0.5$, 1 and 2 MHz.

The half-height of the error signal slope determines the typical 3 dB modulation bandwidth. As shown in Fig. S3, we find the modulation bandwidth of the ACS is aapproximately 4 MHz [13, 14].

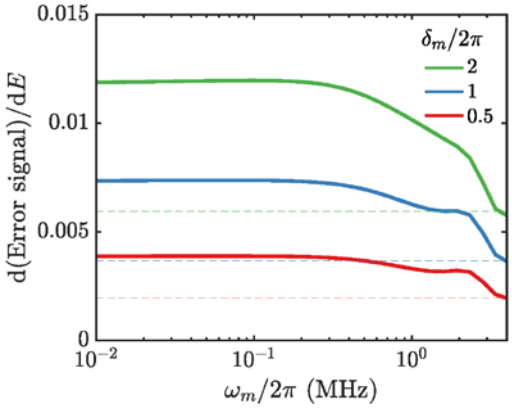

Fig. S3 The slope of the error signal (arbitrary unit) as a function of modulation frequency. The modulation amplitude δ_m of the green, blue and red curves are $2\pi \times 2$ MHz, $2\pi \times 1$ MHz, $2\pi \times 0.5$ MHz, respectively. The horizontal dashed lines marked the half-height of the error signal slopes at low frequency.

Experimental details

Experimental set-up. As shown in Fig. S4, the counter-propagating probe (795 nm) and control (474 nm) lasers excite atoms from ground to Rydberg states. To increase the atomic density, the vapour cell is heated to 60℃, and the corresponding atomic density is approximately 3×10^{11} cm^{-3}(Ref. [15]). The Rydberg EIT spectrum is obtained by scanning the probe laser frequency with a double-passed acousto-optic modulator, and its Doppler background is eliminated by adding a reference beam for balanced detection.

The MW field for Rydberg dressing is produced by a signal generator (R&S SMF 100A) and its amplitude is controlled by a voltage-controlled attenuator (VCA). The MW horn has an operating frequency range from 4 GHz to 40 GHz and an average gain of 13 dB. By placing the horn antenna 40 cm away from the vapor cell, the relative variation of MW field amplitude in vapor cell is reduced to less than 5%. The experimentally detected EIT and EIT-AT spectra with MW off and on are shown in Fig. S4.

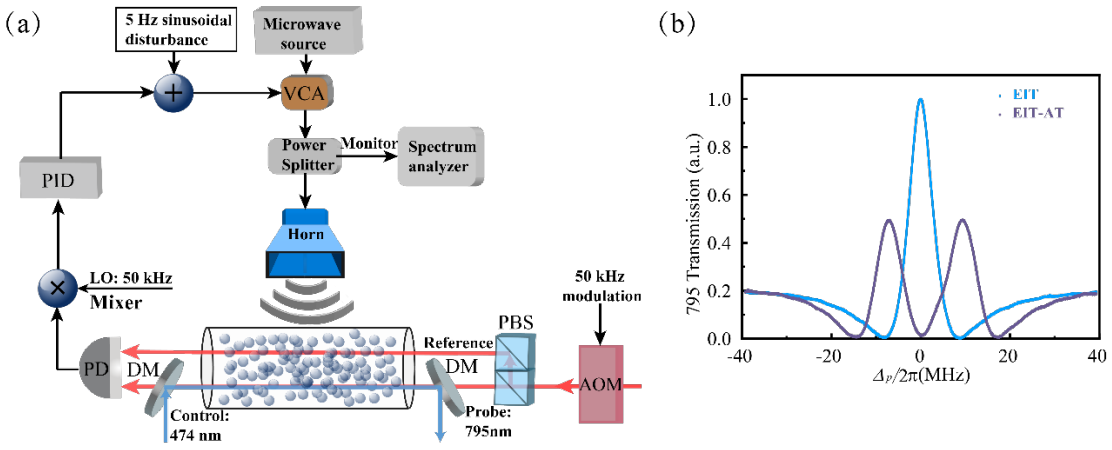

Fig. S4 (a) Detailed schematic diagram of the Rydberg atomic candle. VCA: voltage-controlled attenuator, AOM: acousto-optic modulator, PBS: polarization beam splitter, DM: dichroic mirror, PD: photodiode, PID: the Proportional-Integral-Derivative controller. **(b)** The detected atomic spectra with MW off (EIT) and on (EIT-AT) by a balanced photodiode.

Laser frequency stabilization. The probe laser and the seed of the control laser are frequency-stabilized to a 10-cm-long ultra-low expansion (ULE) cavity. The cavity is coated at both 795 nm and 948 nm with a finesse of 20 000, and the linewidth of the high-finesse cavity is about 75 kHz. The ULE cavity is placed in a vacuum chamber with pressure below 5×10^{-8} Torr, and its temperature is stabilized at zero-crossing point by a temperature control system. The vacuum chamber contains two internal shields to ensure the temperature drift of the cavity < 1 mK/day. Laser frequency stabilization is achieved by the Pound-Drever-Hall (PDH) [16] technique. The absolute frequency of the probe laser is calibrated by an atomic saturation spectrum, and modulated by a fiber electro-optic modulator to match the eigenfrequency of the ULE cavity. Then the two-

photon detuning is calibrated by the EIT spectrum. The resulting uncertainty of the two-photon detuning is about 30 kHz, which is limited by the linewidth of the EIT transmission spectrum.

Determination of MW resonance frequency. To ensure the Rydberg spectrum shifts $\tilde{\Delta}_{\pm}$ are linearly dependent on the MW Rabi frequencies Ω_{MW}, the detuning between MW field and the Rydberg transition δ_{MW}, needs to be minimized. Otherwise, the frequency interval Δf_{δ} between the MW-dressed Rydberg states will not equal to the Rabi frequency Ω_{MW} any more, the relation becomes: $\Delta f_{\delta} = \sqrt{(\delta_{MW})^2 + (\Omega_{MW})^2}$. Besides, the frequency shifts of the dressed states will be asymmetric, which are $\tilde{\Delta}_{\pm} = \delta_{MW}/2 \pm \sqrt{(\delta_{MW})^2 + (\Omega_{MW})^2}/2$ (Ref. [1]). The MW detuning can be obtained as $\delta_{MW} = \tilde{\Delta}_{+} + \tilde{\Delta}_{-}$. In this work, δ_{MW} is reduced to less than 0.1 MHz by equalizing the frequency shifts of the $|+\rangle$ and $|-\rangle$ dressed states.

Deviation of the stabilized field amplitude. The ability to stabilize MW field amplitude at a target value is an important feature of the atomic candle. But physical processes that shift the transmission spectrum could cause deviations from target MW field amplitude. The frequency deviations of probe and control lasers directly change the two-photon detuning, which determines the stabilized MW field amplitude. The two-photon resonant frequency f_0 is determined by EIT spectrum. Due to the limitation from the linewidth of the EIT spectrum, the uncertainty of resonant frequency is about 30 kHz, and the corresponding uncertainty of MW field amplitude is $0.05\ \mathrm{mV \cdot cm^{-1}}$.

Another factor causes the amplitude deviation is the MW detuning δ_{MW}, as a result of which, the frequency interval Δf_{δ} is not equal to the MW Rabi frequency Ω_{MW}. The frequency shift of the dressed states can be measured by the EIT and AT spectra, with the relationship: $\tilde{\Delta}_{\pm} = f_{\pm} - f_0$, where $f_{\pm}$is the two-photon resonant frequencies corresponding to the MW-dressed states $|\pm\rangle$. The standard deviation of MW detuning is $\sqrt{6} \times 30$ kHz, which results from the frequency uncertainties of $f_i (i$ stands for $\pm$ and 0). The deviation of stabilized MW field amplitude caused by the MW detuning is negligible, even for the minimum MW field amplitude, the deviation is 4 orders of magnitude lower than the target amplitude.

In summary, the MW field amplitude can be stabilized at a target value with a standard deviation $0.05\ \mathrm{mV \cdot cm^{-1}}$.

Frequency domain analysis of stabilization efficacy. When a 5 Hz sinusoidal disturbance is added to the MW field amplitude, the stabilization efficacy of the Rydberg atomic candle in time domain is shown in the main text. Due to the limitation of stabilization bandwidth, the feedback control efficacy varies with disturbance frequency. In order to investigate the stabilization efficacy at 5 Hz, the frequency domain information of the MW field amplitude is obtained by a fast Fourier transform (FFT) of the MW field amplitude measured in time domain, as shown in Fig. S5. For the 5 Hz component, the signal amplitude is suppressed by more than 3 orders of magnitude with the feedback control loop closed.

The stabilization efficacy at 5 Hz (with different operating frequencies) is shown in the main text. Since the modulation frequency at 50 kHz is relatively high, disturbance with higher frequency can be stabilized by the Rydberg atomic candle. As shown in Fig. S6, for 100 Hz disturbance, the MW field amplitude fluctuation is suppressed by 76 times at 14.8 GHz. The stabilization bandwidth depends on the modulation frequency, which is only limited by the response rate of the EIT spectrum for a Rydberg atomic candle [13].

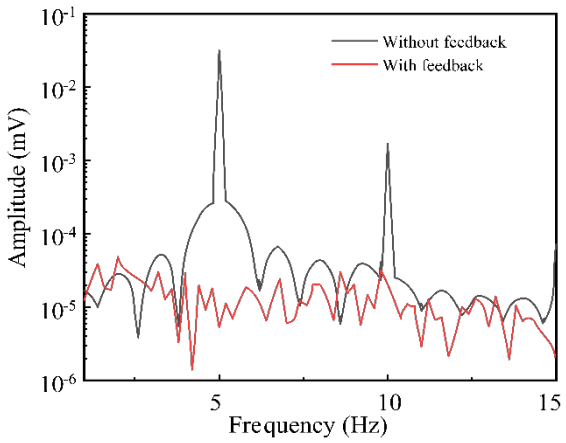

Fig. S5 Frequency domain analysis with feedback loop open and closed.

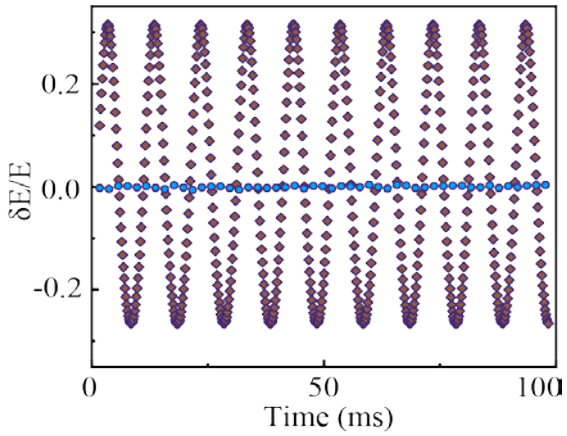

Fig. S6 Stabilization efficacy with a 100 Hz disturbance.

References

1. M. Fleischhauer, A. Imamoglu, and J.P. Marangos, Electromagnetically induced transparency: Optics in coherent media, *Rev. Mod. Phys*. 77(2), 633 (2005)
2. M. Fleischhauer and M.D. Lukin, Dark-state polaritons in electromagnetically induced transparency, *Phys. Rev. Lett*. 84(22), 5094 (2000)
3. M. Tanasittikosol, J.D. Pritchard, D. Maxwell, A. Gauguet, K.J. Weatherill, R.M. Potvliege, and C.S. Adams, Microwave dressing of Rydberg dark states, *J. Phys. B* 44(18), 184020 (2011)
4. R.F. Gutterres, C. Amiot, A. Fioretti, C. Gabbanini, M. Mazzoni, and O. Dulieu, Determination of the ^{87}Rb 5p state dipole matrix element and radiative lifetime from the photoassociation spectroscopy of the $Rb_2 0_g^-$ (P3/2) long-range state, *Phys. Rev. A* 66(2), 024502 (2002)
5. N. Šibalić, J.D. Pritchard, C.S. Adams, and K.J. Weatherill, ARC: An open-source library for calculating properties of alkali Rydberg atoms, *Comput. Phys. Commun*. 220, 319 (2017)
6. E.J. Robertson, N. Šibalić, R.M. Potvliege, and M.P.A. Jones, ARC 3.0: An expanded Python toolbox for atomic physics calculations, *Comput. Phys. Commun*. 261, 107814 (2021)
7. U. Volz and H. Schmoranzer, Precision lifetime measurements on alkali atoms and on helium by beam–gas–laser spectroscopy, *Phys. Scr*. T65, 48 (1996)
8. U. Raitzsch, R. Heidemann, H. Weimer, B. Butscher, P. Kollmann, R. Löw, H.P. Büchler, and T. Pfau, Investigation of dephasing rates in an interacting Rydberg gas, *New J. Phys.* 11(5), 055014 (2009)
9. H. Zhang, L. Zhang, L. Wang, S. Bao, J. Zhao, S. Jia, and G. Raithel, Autler-Townes spectroscopy with interaction-induced dephasing, *Phys. Rev. A* 90(4), 043849 (2014)
10. L. Hao, Y. Jiao, Y. Xue, X. Han, S. Bai, J. Zhao, and G. Raithel, Transition from electromagnetically induced transparency to Autler–Townes splitting in cold cesium atoms, *New J. Phys.* 20(7), 073024 (2018)
11. D. Yan, B. Wang, Z. Bai, and W. Li, Electromagnetically induced transparency of interacting Rydberg atoms with two-body dephasing, *Opt. Express*. 28(7), 9677 (2020)
12. N.J.B. Green, Chapter 8 - Steady-state master equation methods, in: Comprehensive Chemical Kinetics, ed. S.H. Robertson, 2019, Elsevier, pp 465-514
13. M.T. Simons, A.H. Haddab, J.A. Gordon, and C.L. Holloway, A Rydberg atom-based mixer: Measuring the phase of a radio frequency wave, *Appl. Phys. Lett.* 114(11), 114101 (2019)
14. D.H. Meyer, K.C. Cox, F.K. Fatemi, and P.D. Kunz, Digital communication with Rydberg atoms and amplitude-modulated microwave fields, *Appl. Phys. Lett.* 112(21), 211108 (2018).
15. W.M. Haynes, CRC Handbook of Chemistry and Physics. 2014: CRC Press
16. E.D. Black, An introduction to Pound–Drever–Hall laser frequency stabilization, *Am. J. Phys.* 69(1), 79-87 (2000)